Supplemental Information File for

Variations of dissolved greenhouse gases (CO_2, CH_4, N_2O) in the Congo River overwhelmingly driven by fluvial-wetland connectivity

Alberto V. Borges[1,*], François Darchambeau[1,**], Thibault Lambert[1,***], Cédric Morana[2], George Allen[3], Ernest Tambwe[4], Alfred Toengaho Sembaito[4], Taylor Mambo[4], José Nlandu Wabakhangazi[5], Jean-Pierre Descy[1], Cristian R. Teodoru[2,****], Steven Bouillon[2]

[1] Chemical Oceanography Unit, University of Liège, Liège, Belgium
[2] Department of Earth and Environmental Sciences, KULeuven, Leuven, Belgium
[3] Department of Geography, Texas A&M University, USA
[4] Université de Kisangani, Centre de Surveillance de la Biodiversité, DRC Congo
[5] Congo Atomic Energy Commission, Kinshasa, DRC Congo

[*] alberto.borges@uliege.be
** Present address: Direction générale opérationnelle Agriculture, Ressources naturelles et Environnement, Service Publique de Wallonie, Belgium
*** Present address: University of Lausanne, Institute of Earth Surface Dynamics, Lausanne, Switzerland
**** Present address: Eidgenössische Technische Hochschule Zürich, Switzerland.

Table S1: Annual average freshwater discharge of the main tributaries (>300 $m^3 s^{-1}$) of the Congo (Rodier 1983).

River name	Left/right bank	Freshwater discharge ($m^3 s^{-1}$)
Lobaye	Left bank	355
Itimberi	Right bank	356
Lefini	Right bank	388
Alima	Right bank	575
Lindi	Right bank	1200
Lomami	Left bank	1214
Sangha	Right bank	1715
Aruwimi	Left bank	2200
Ruki	Left bank	4200
Oubangui	Right bank	4340
Lualaba	-	6400
Kwa	Left bank	11320

Figure S1: Comparison of the partial pressure of CO_2 (pCO_2 in ppm) measured in the home laboratory by gas chromatography (GC) from serum bottles poisoned with $HgCl_2$ (+$HgCl_2$ & GC) with the pCO_2 measured directly in the field with an infra-red gas analyzer (IRGA, in most cases a Li-Cor Li-840) (direct & IRGA) as function of total alkalinity (TA in µmol kg^{-1}) and as function of pCO_2 (direct & IRGA) in the Congo River during high water (03/12/2013-19/12/2013) and falling water (10/06/14-30/06/14) periods. The increase of pCO_2 (+$HgCl_2$ & GC) compared to pCO_2 (direct & IRGA) is attributed to the precipitation of $HgCO_3$ that leads to a shift of equilibrium of HCO_3^- towards CO_2 (Hg^{2+} + $2HCO_3^-$ = $HgCO_3$ + CO_2 + H_2O). This is consistent with the increase of the difference between pCO_2 (+$HgCl_2$ & GC) and pCO_2 (direct & IRGA) with TA that mainly corresponds to HCO_3^- in freshwater. As the highest pCO_2 values are observed in blackwaters with low to nil TA values, the difference between pCO_2 (+$HgCl_2$ & GC) (direct & IRGA) is highest at low pCO_2 (direct & IRGA) values.

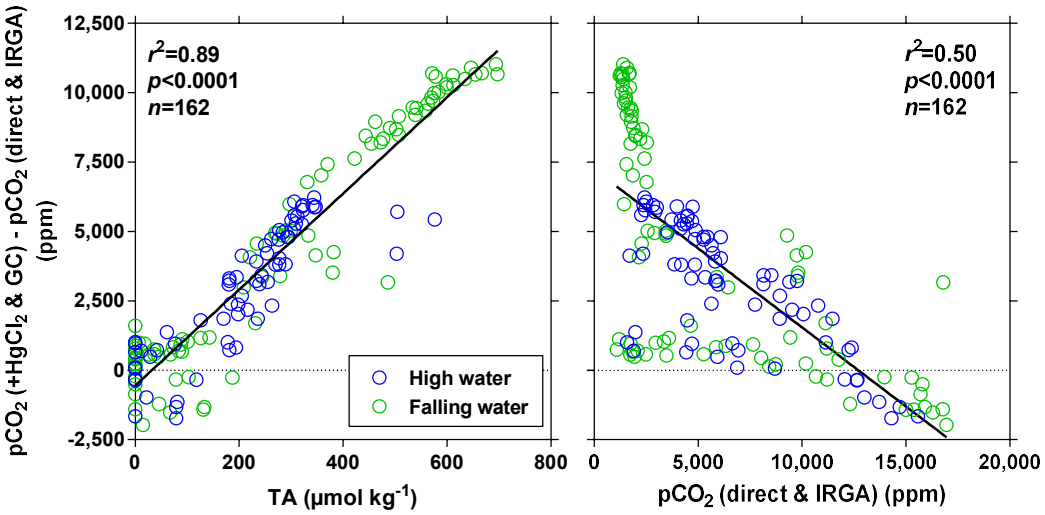

Figure S2: Comparison of measurements of turbidity with the YSI 6600 multiparameter probe (nephelometric turbidity unit (NTU)) and discrete total suspended matter (TSM in mg L^{-1}) in the Congo River during high water (03/12/2013-19/12/2013) and falling water (10/06/14-30/06/14) periods.

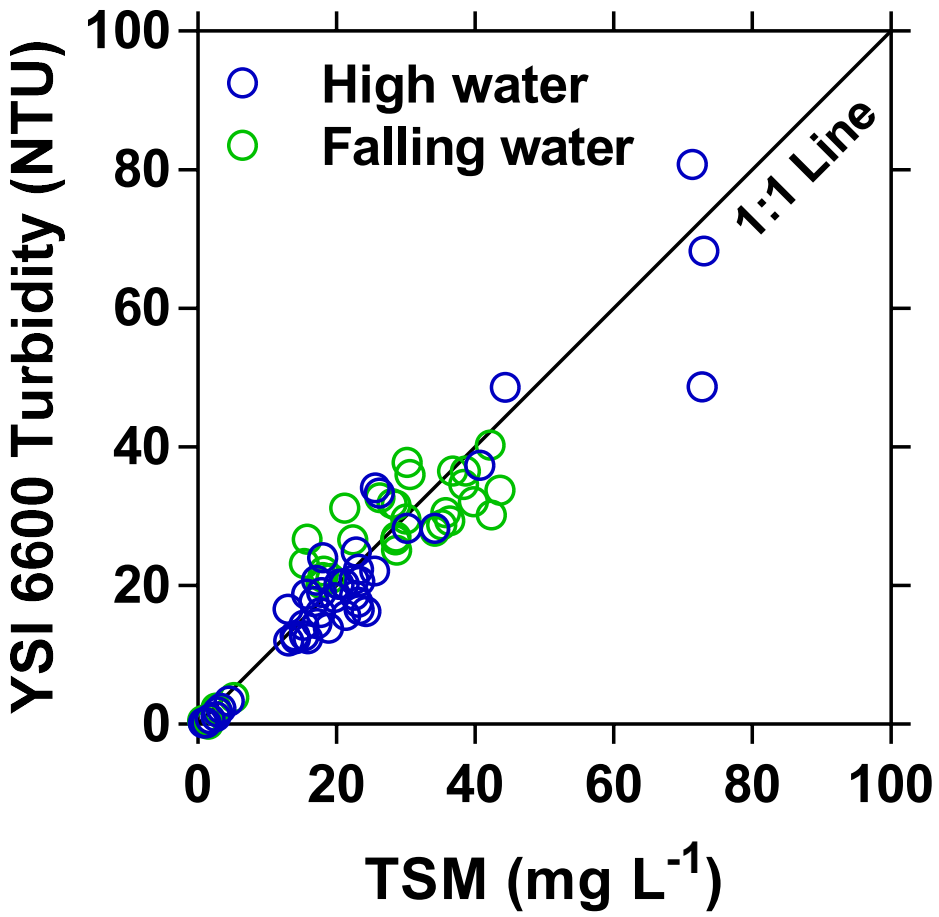

Figure S3: Comparison of measured and modelled primary production (mmol m^{-2} d^{-1}). Data points corresponding to Chlorophyll-*a* concentrations < 0.3 µg L^{-1} are shown by red dots. Solid line corresponds to 1:1 line and dotted line corresponds to the linear regression.

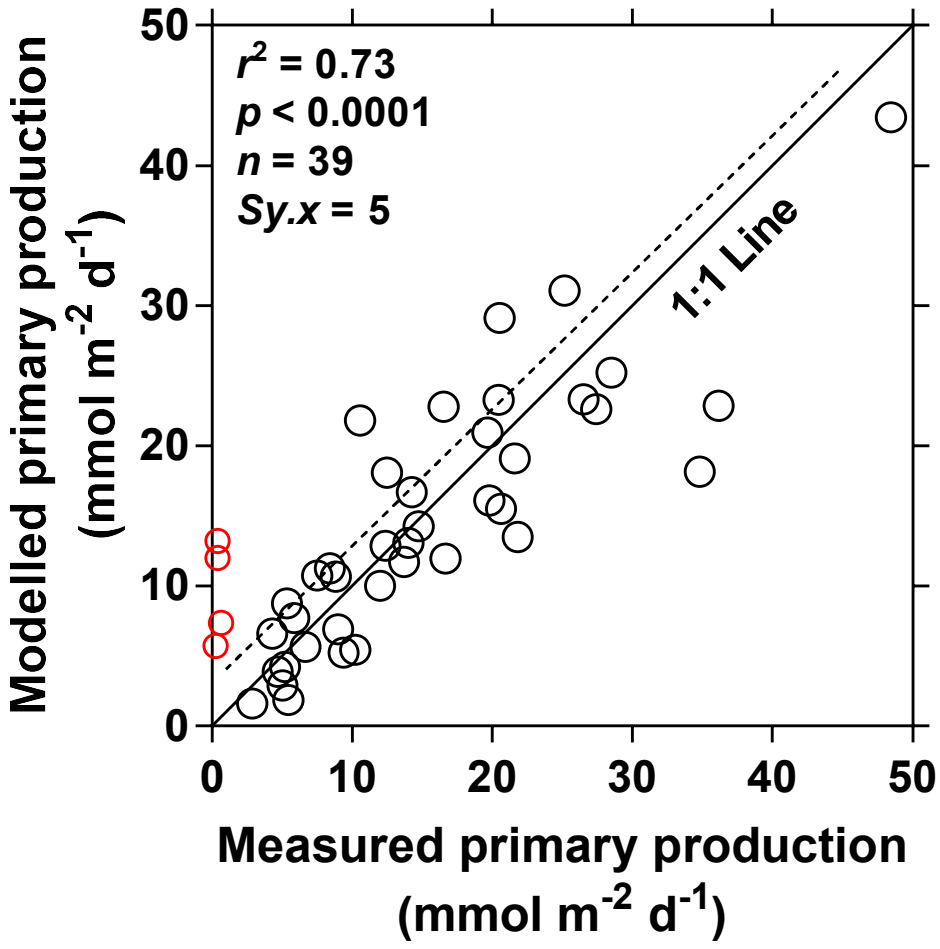

Figure S4: Partial pressure of CO_2 (pCO_2 in ppm) as function of dissolved O_2 saturation level ($\%O_2$ in %), total suspended matter (TSM in mg L^{-1}), pH and specific conductivity in the Congo River during high water (03/12/2013-19/12/2013, *n*=10,505) and falling water (10/06/14-30/06/14, *n*=12,968) periods.

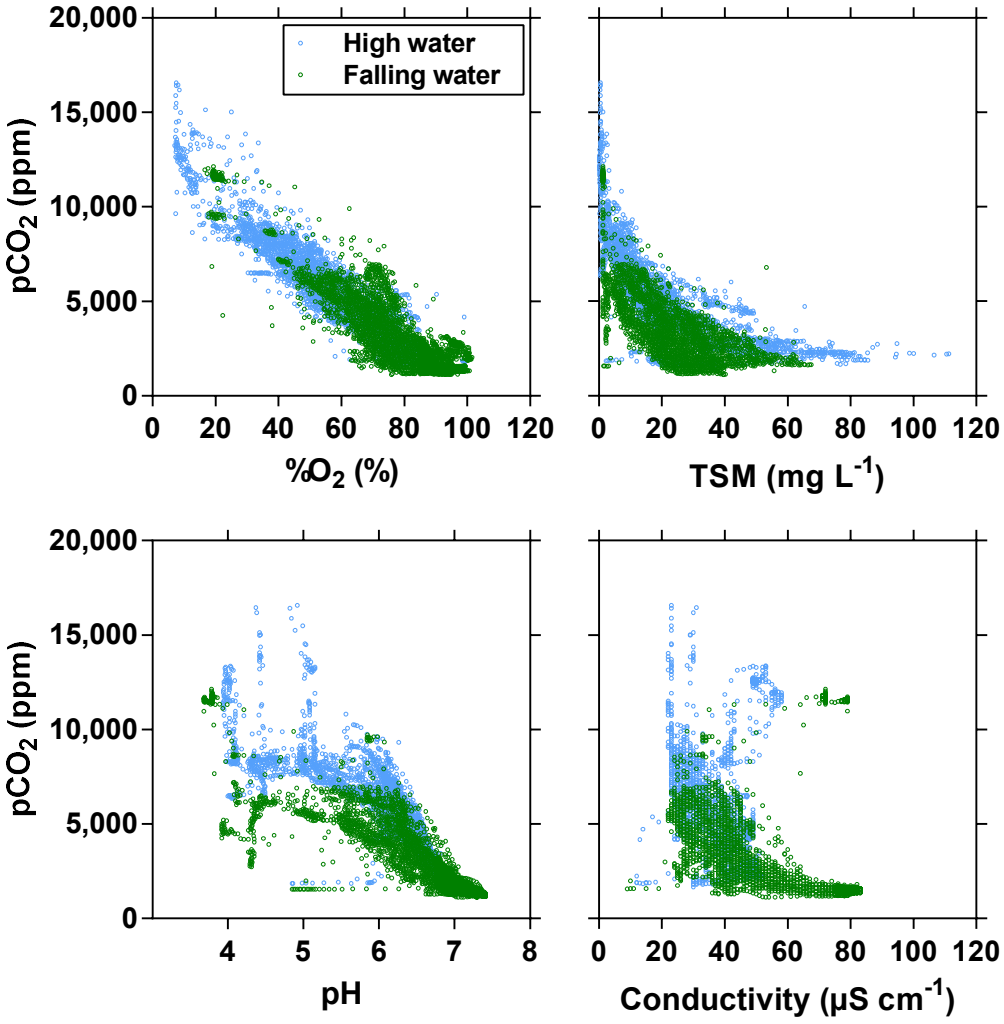

Figure S5: Fraction of oxidized CH_4 computed from the carbon stable isotope composition of CH_4 in surface waters of mainstem of the Congo River (black symbols) and tributaries (green symbols) as a function of dissolved CH_4 concentration (nmol L^{-1}) and as function of the distance upstream of Kinshasa, obtained along a longitudinal transect along the Congo River from Kisangani (10/06/14-30/06/14). Dotted line indicates linear regression.

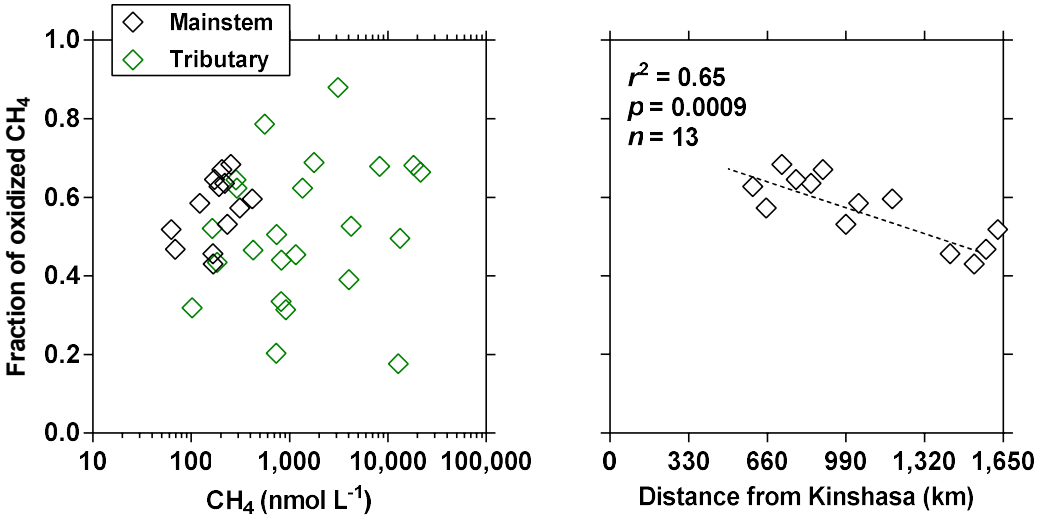

Figure S6: Photographs of several macrophytes present in the Congo River network. Photo credits AV Borges and F Darchambeau.

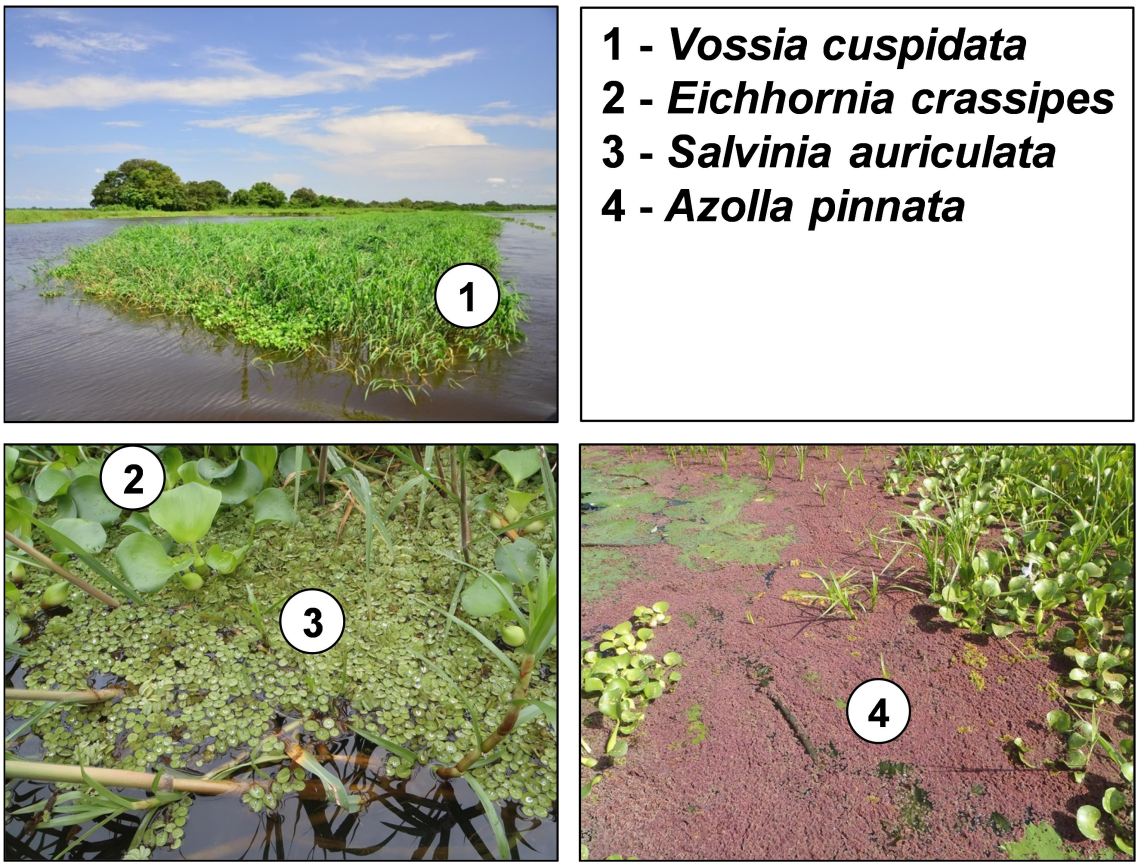

Figure S7: CH_4 oxidation rates (nmol L^{-1} d^{-1}) as a function of dissolved CH_4 concentration (nmol L^{-1}) in several sites of the Congo River network (16/04/15-06/05/15)

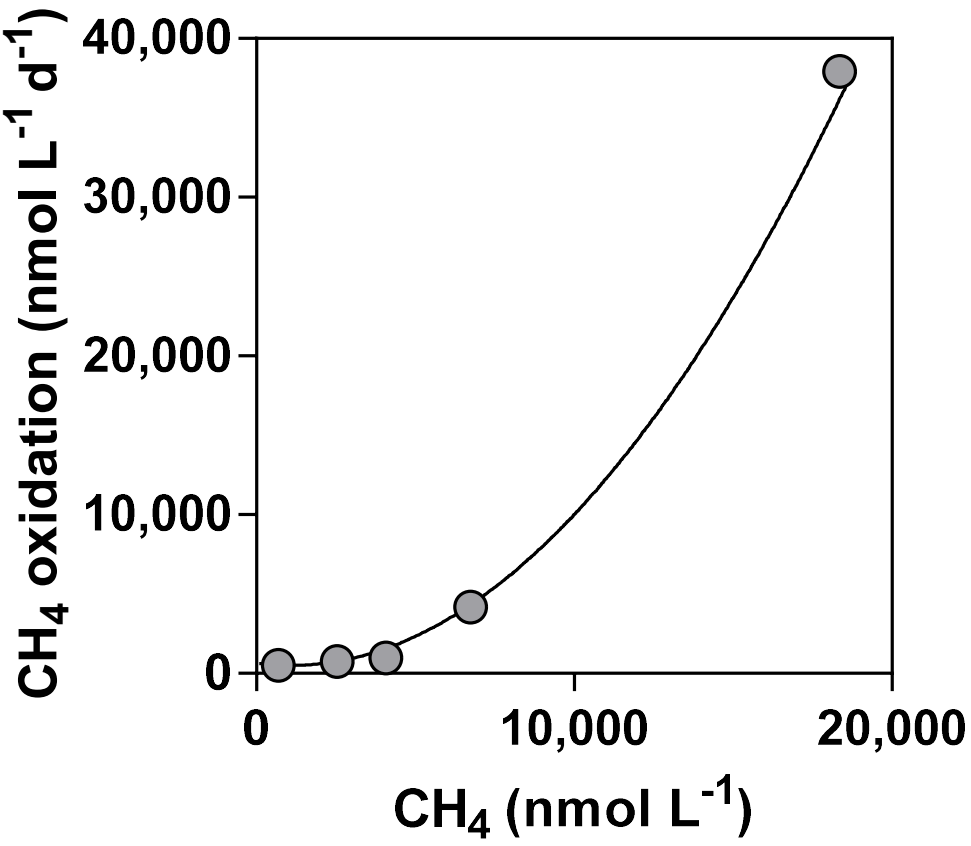

Figure S8: True colour remote sensed images (Google Earth) of the confluence of the Congo River mainstem with the Itimbiri andRuki Rivers and outlet of Lake Tumba.

Figure S9: Photographs of *Vossia cuspidata* meadows at the mouth of the Ruki (top) and in the Congo mainstem (bottom). Photo credits AV Borges

Figure S10: Comparison of the partial pressure of CO_2 (pCO_2 in ppm), dissolved oxygen concentration (O_2 in µmol L^{-1}), water temperature and specific conductivity (µS cm^{-1}) acquired at the anchoring site on shore (typically around 17h00 universal time (UT), just before dusk, “Afternoon”) with the data on the same spot the next day (typically around 04h30 UT, just after dawn, “Morning”). Red dots were excluded from the statistical test.

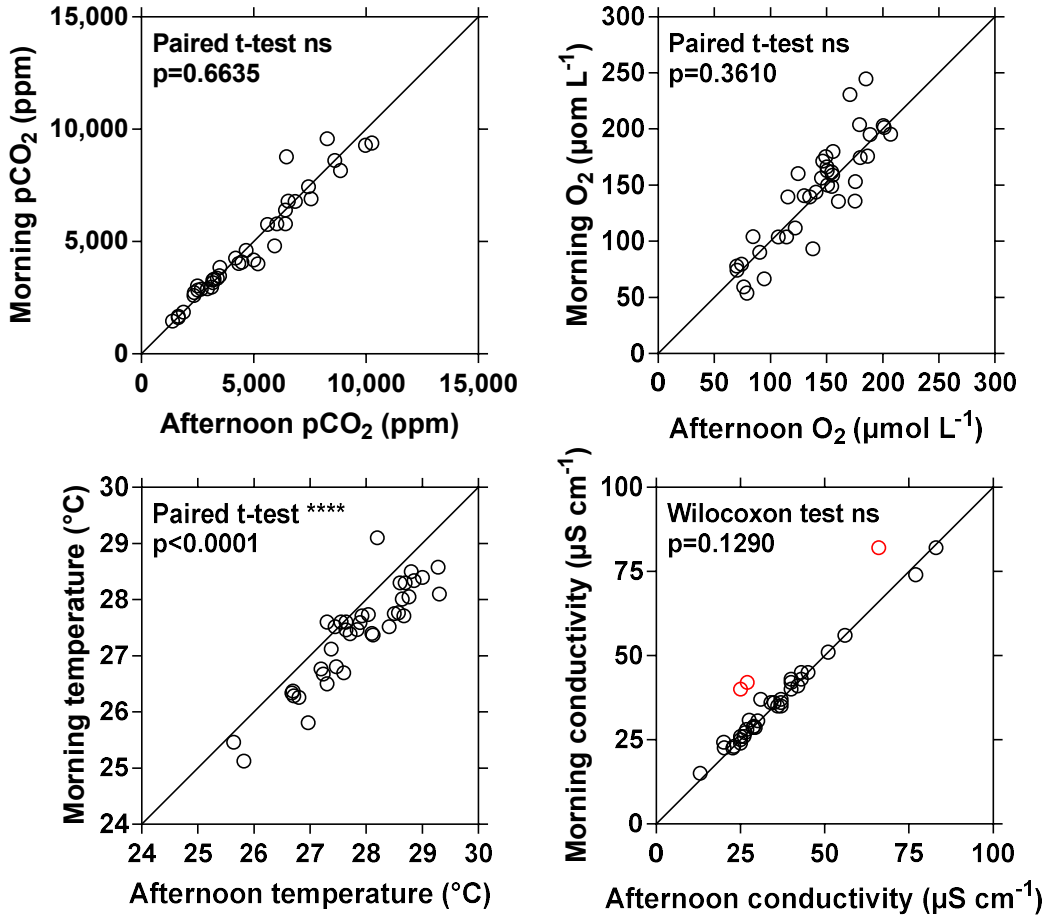

Figure S11: Carbon stable isotope composition of dissolved inorganic carbon (DIC) (δ^{13}C-DIC in ‰) for a total alkalinity (TA) to DIC ratio (µmol:µmol) equal to zero in surface waters of the Congo River network as a function of the fraction of C_4 vegetation on the catchment based on the geospatial model of Still and Powell (2010) and the fraction of savannah on the catchment extracted from Global Land Cover 2009.

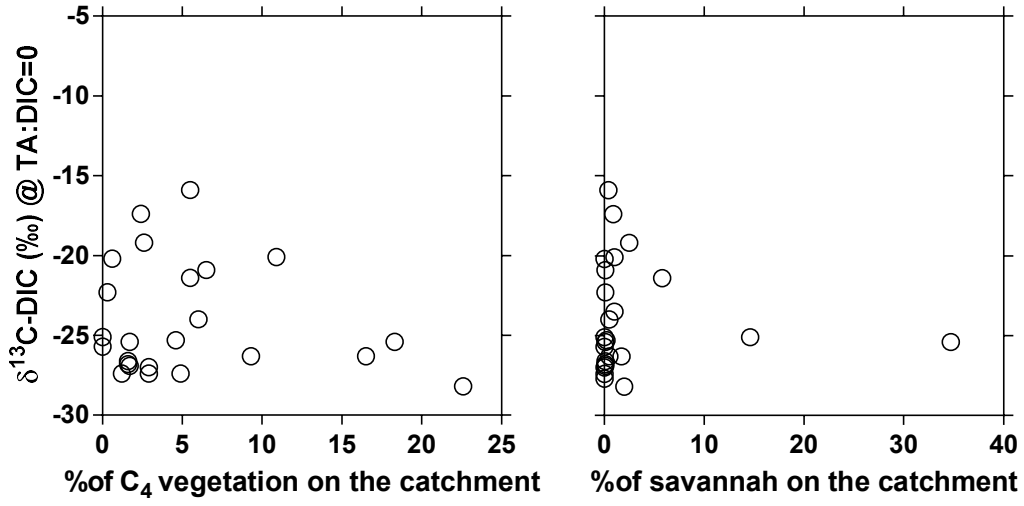

Figure S12: Annual average of dissolved N_2O saturation level (%N_2O in %), freshwater discharge (m^3 s^{-1}) and water temperature (°C) in the Congo River mainstem at Kisangani (2013-2017).

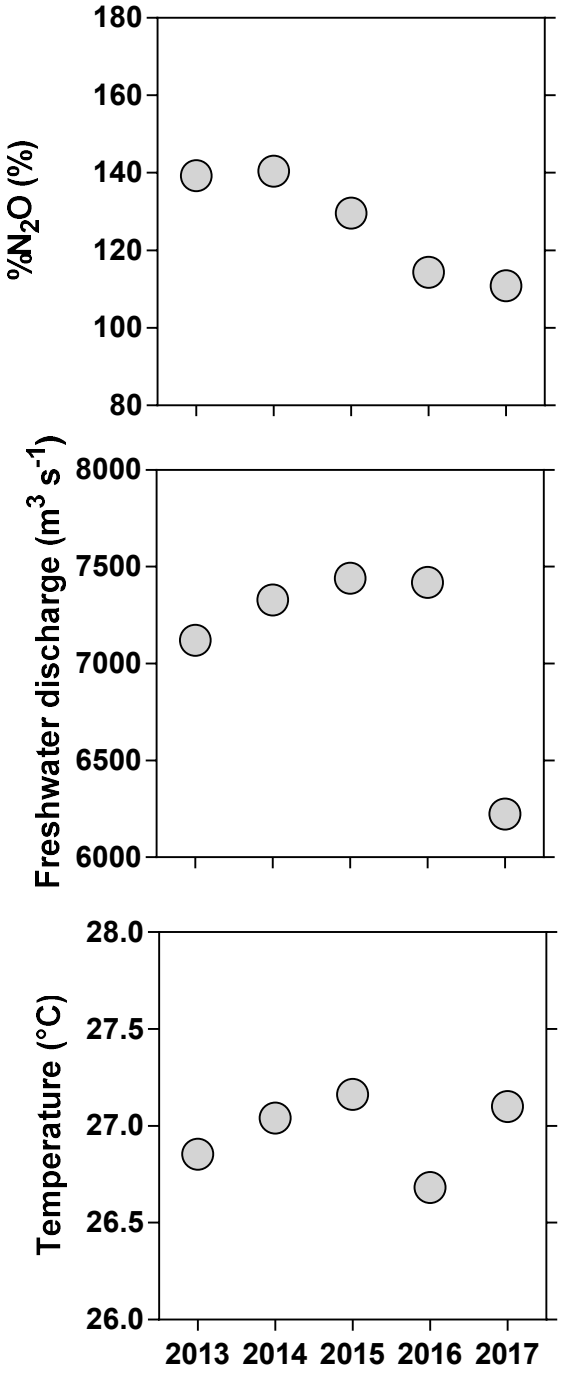

Figure S13: Partial pressure of CO_2 (pCO_2 in ppm) as a function of freshwater discharge ($m^3\ s^{-1}$) in the Congo River mainstem at Kisangani (2017-2018).

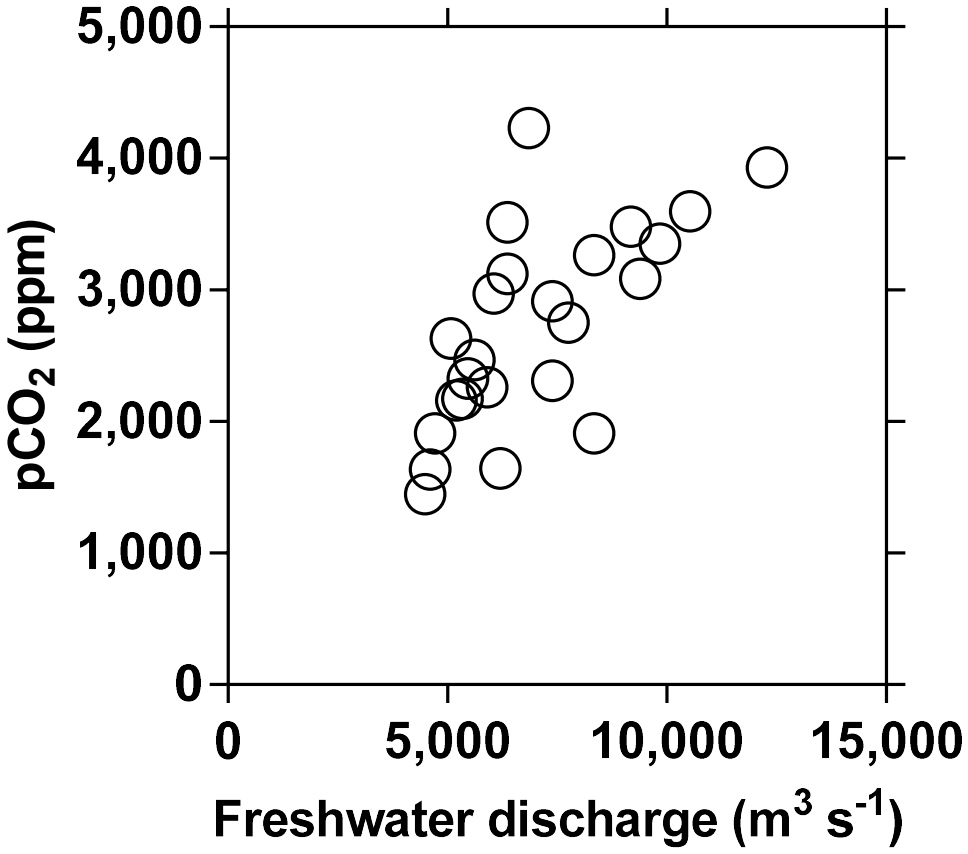

Figure S14: Variation of median gas transfer velocity (k_{600} in cm h^{-1}) and stream surface area (km^2) as a function of Strahler stream order in the Congo River network.

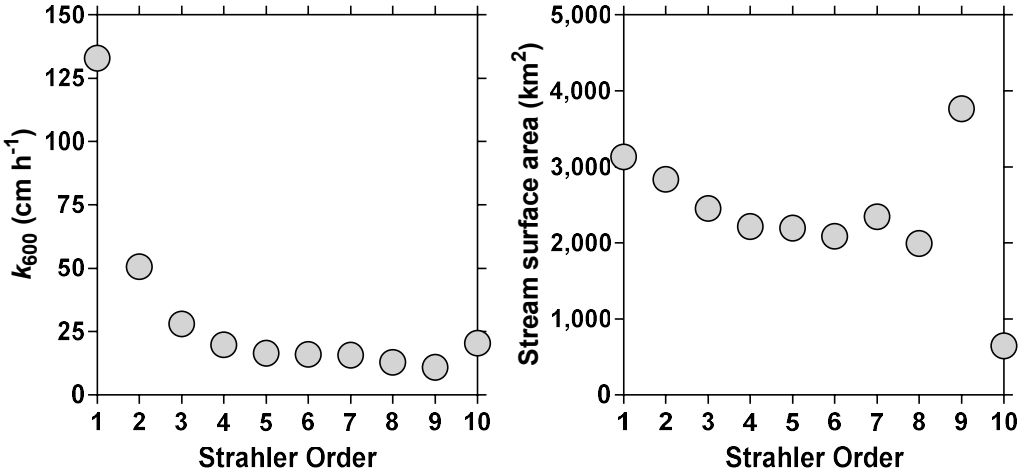

Figure S15: Median partial pressure of CO_2 (pCO_2 in ppm), CH_4 concentration (nmol L^{-1}) and N_2O (nmol L^{-1}) as a function of Strahler stream order in the Congo River network for rivers and streams draining and not draining the Cuvette Centrale Congolaise. Data for order 1 were extrapolated either by considering the same value as for order 2 or with a linear regression (dotted lines).

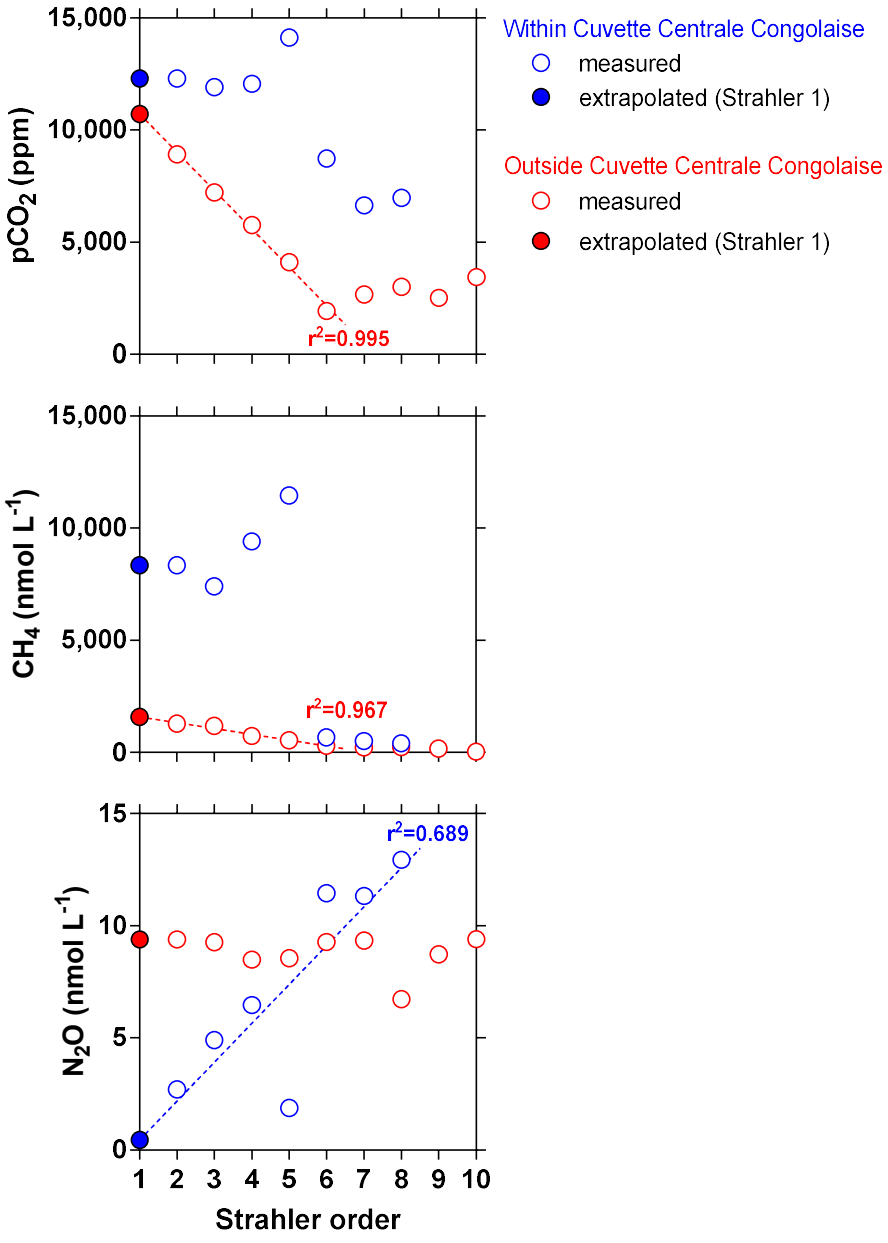

Figure S16: Air-water fluxes of CO_2 (FCO_2 in mmol m^{-2} d^{-1}), of CH_4 (FCH_4 in µmol m^{-2} d^{-1}), of N_2O (FN_2O in µmol m^{-2} d^{-1}) in the Lualaba at Kisangani as a function of freshwater discharge (m^3 s^{-1}). Fluxes were computed as explained in the material and methods section from flow velocity derived from freshwater discharge with the hydraulic equation given by Raymond et al. (2012). Dotted lines indicate linear regression.

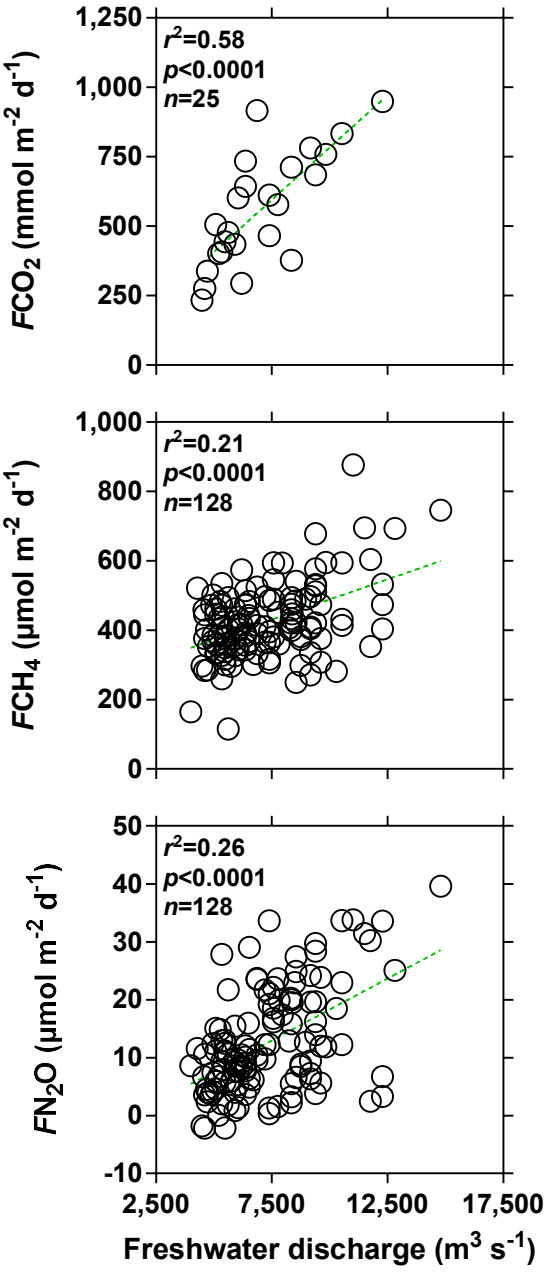

Figure S17: Field data of the partial pressure of CO_2 (pCO_2 in ppm) in tributaries (green symbols) and mainstem (black symbols) of the Congo River (03/12/2013-19/12/2013, 10/06/14-30/06/14), and the output of the model of Lauerwald et al. (2015) at proximity of the sampled sites as function of longitude (°E), as well as the average basin-wide pCO_2 value for the Congo River used by Raymond et al. (2013). Box plot of pCO_2 in surface waters of rivers and streams of the Congo River network draining and not draining the Cuvette Centrale Congolaise from field measurements (03/12/2013-19/12/2013; 10/06/14-30/06/14) and the output of the model of Lauerwald et al. (2015) (orange dots). Field data (both mainstem and tributaries, blue) were significantly higher than model output (red) (Mann-Whitney, p=0.0119) for systems draining the Cuvette Centrale Congolaise but significantly lower than model output (Mann-Whitney, p=0.0044) for systems outside the Cuvette Centrale. The box represents the first and third quartile, horizontal line corresponds to the median, the cross to the average, error bars correspond to the maximum and minimum, symbols show all data points. Although the model of Lauerwald et al. (2015) provides pCO_2 values that are more consistent with observations than the basin-wide average value used by Raymond et al. (2013), the model fails to represent the increase of pCO_2 in rivers draining the Cuvette Centrale Congolaise. This statistical model predicts the fluvial pCO_2 from the net primary production on *terra firme* (as well as slope, air temperature and population density), so fails to account for the influence from wetland carbon inputs.

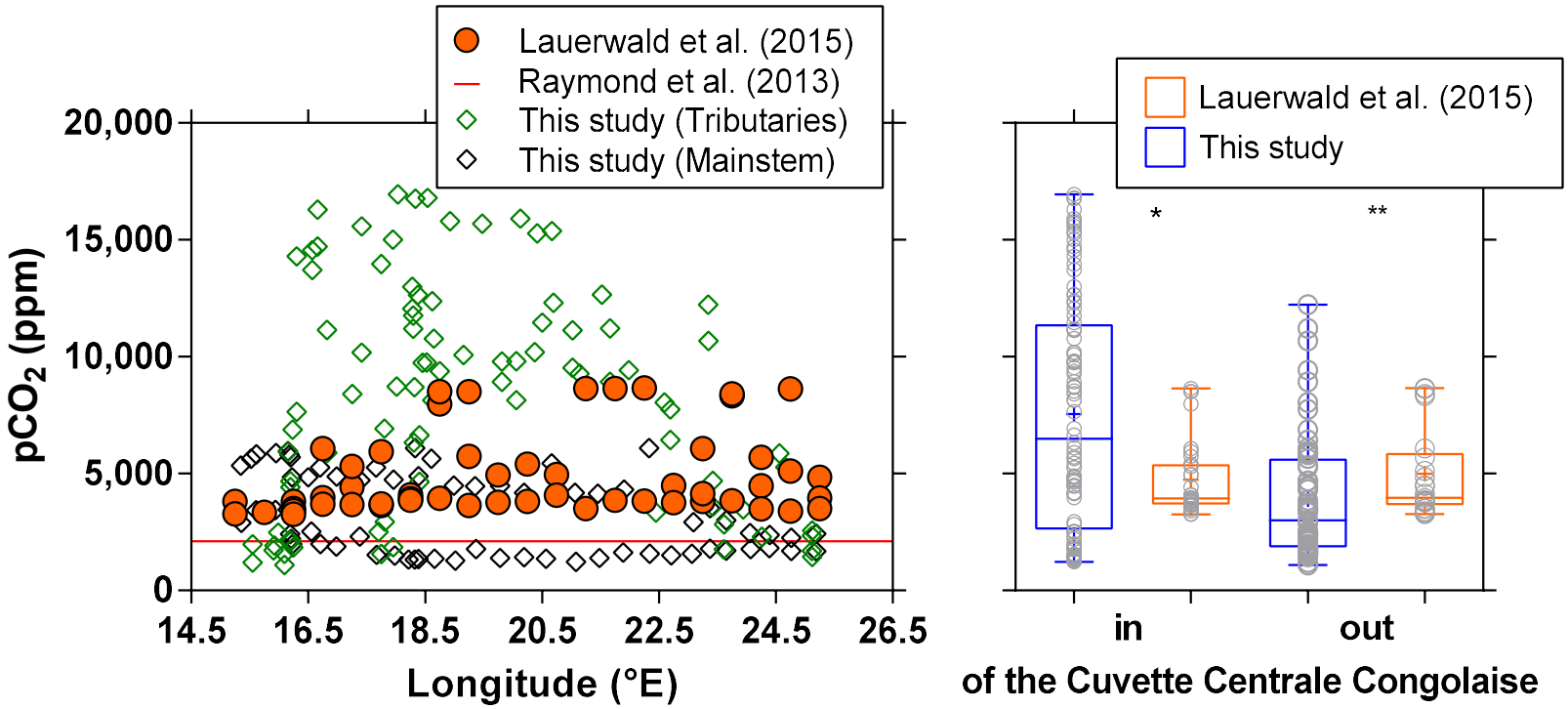

References

Lauerwald, R., Laruelle, G. G., Hartmann, J., Ciais, P., and Regnier, P. A. G.: Spatial patterns in CO2 evasion from the global river network, Global Biogeochem. Cycles, 29, 534-554, doi:10.1002/2014GB004941, 2015.

Raymond, P. A., Hartmann, J., Lauerwald, R., Sobek, S., McDonald, C., Hoover, M., Butman, D., Striegl, R., Mayorga, E., Humborg, C., Kortelainen, P., Dürr, H., Meybeck, M., Ciais, P., and Guth, P.: Global carbon dioxide emissions from inland waters, Nature, 503, 355-359, 10.1038/nature12760, 2013.

Raymond, P. A., Zappa, C. J., Butman, D., Bott, T. L., Potter, C., Mulholland, P., Laursen, A. E., McDowell, W. H., and Newbold, D.: Scaling the gas transfer velocity and hydraulic geometry in streams and small rivers. Limnol. Oceanogr. Fluids Environ., 2, 41-53, doi: 10.1215/21573689-1597669, 2012.

Rodier, J. A.: Aspects scientifiques et techniques de l'hydrologie des zones humides de l'Afrique centrale, Hydrology of Humid Tropical Regions with Particular Reference to the hydrological Effects of Agriculture and Forestry Practice (Proceedings of the Hamburg Symposium, August 1983), IAHS Publ. no. 140, 1983.

Still, C. J., and Powell, R. L.: Continental-scale distributions of vegetation stable carbon isotope ratios. West JB, Bowen GJ, Dawson TE, Tu KP, editors. Isoscapes. Netherlands: Springer Netherlands. p179-193, 2010.